Journal of Materials Chemistry

Cite this: *J. Mater. Chem.*, 2012, **22**, 11950

www.rsc.org/materials

PAPER

Highly ordered tailored three-dimensional hierarchical nano/microporous gold–carbon architectures

Sirilak Sattayasamitsathit,[a] Aoife M. O'Mahony,[a] Xiaoyin Xiao,[b] Susan M. Brozik,[b] Cody M. Washburn,[b] David R. Wheeler,[b] Wei Gao,[a] Shelley Minteer,[c] Jennifer Cha,[a] D. Bruce Burckel,[b] Ronen Polsky*[b] and Joseph Wang*[a]

Received 10th March 2012, Accepted 13th April 2012
DOI: 10.1039/c2jm31485a

The preparation and characterization of three-dimensional hierarchical architectures, consisting of monolithic nanoporous gold or silver films formed on highly ordered 3D microporous carbon supports, are described. The formation of these nano/microporous structures involves the electrodeposition or sputtering of metal alloys onto the lithographically patterned multi-layered microporous carbon, followed by preferential chemical dealloying of the less noble component. The resulting hierarchical structure displays a highly developed 3D interconnected network of micropores with a nanoporous metal coating. Tailoring the nanoporosity of the metal films and the diameter of the large micropores has been accomplished by systematically changing the alloy compositions *via* control of the deposition potential, plating solution and coarsening time. SEM imaging illustrates the formation of unique biomimetic nanocoral- or nanocauliflower-like self-supporting structures, depending on the specific preparation conditions. The new 3D hierarchical nano/microporous architectures allow for enhanced mass transport and catalytic activity compared to common nanoporous films prepared on planar substrates. The functionality of this new carbon–gold hierarchical structure is illustrated for the greatly enhanced performance of enzymatic biofuel cells where a substantially higher power output is observed compared to the bare microporous carbon substrate.

1. Introduction

Micro- and nanoporous structures have attracted considerable recent interest due to their remarkable chemical/physical properties.[1–4] In particular, three-dimensional (3D) structures of micro- and nanoscale materials have received enormous attention owing to a wide range of potential applications, including energy storage,[5] plasmonics,[6] sensing[7,8] and catalysis.[9,10]

Here we describe the first example of a 3D hierarchical porous carbon–gold architecture based on a judicious combination of micro- and nanostructures: new interferometric lithographically fabricated 3D microporous carbon[11,12] and nanoporous Au or Ag films.[3,4,13] Within this new hierarchical architecture, we can tailor both the microporosity of the carbon substrate (indirectly by varying the thickness of the alloy film) and the nanoporosity of the porous gold film (by modifying the deposition and dealloying conditions). Such fine tuning of both the micro/submicrometre-sized building blocks and the nanometre-sized assemblies of the resulting hierarchical architectures leads to great versatility towards diverse applications.

The lithographically fabricated 3D porous materials (used in the present work and developed recently at Sandia National Laboratory) display an attractive highly ordered open-porous carbon microstructure to support the nanoporous metal films.[11,12] The open-cell morphology and structural regularity of these multilayered microporous carbons offer many structural and hydrodynamic advantages such as a facile support for catalytic nanoparticles and diffusion profiles that lead to enhanced internal mass transport within the structures.[12] Coating this 3D highly periodic microporous carbon substrate with nanoporous metal layers, through electrodeposition of alloys and dealloying these metal films, provides a high-area catalytic metal surface with nanoscale pore structures and high surface-to-volume ratios.

Such nanoporous metal layers are commonly prepared on 2D substrates *via* electrodeposition of a single-phase two-component alloy $M1_XM2_{1-X}$ followed by electrochemical or chemical etching of the less noble component.[3,4,13,14] Ding and Erlebacher[4] combined nano- and micro-porous Au films using a two-dimensional substrate. The present work, in contrast, aims at producing a 3D hierarchical structure of micropores and

[a]*Department of Nanoengineering, University of California, San DiegoLa Jolla, CA, 92093 USA. E-mail: josephwang@ucsd.edu*
[b]*Sandia National Laboratories, Department of Biosensors and Nanomaterials, PO Box 5800, Albuquerque, NM 87185, USA. E-mail: rpolsky@sandia.gov*
[c]*Department of Chemistry and Materials Science and Engineering, University of Utah, Salt Lake City, UT 84112, USA*

nanopores with well-defined repeated micro-periodicity by preparing a nanoporous gold film over the lithographically fabricated multi-layered microporous carbon substrate.

The preparation of the new nano/micro-hierarchical metal–carbon architectures relies on the electrodeposition or sputtering of a binary alloy, Au–Ag or Ag–Al, onto the microporous carbon support followed by preferential etching of the Ag or Al sacrificial metal, respectively (Fig. 1). Control of the microporosity is achieved through different rates of the gold-reordering during the etching and coarsening step for different levels of the sacrificial metal. Consequently, alloy segments with a lower gold content lead to thinner nanoporous layers and thus to larger micropores of the overall scaffold. The combination of electrodeposition of the alloy onto the 3D microporous carbon with the preferential dealloying processes thus results in an attractive route for preparing tailor-made highly ordered hierarchical architectures, resembling nanocoral- or nanocauliflower-like structures. Such new structures combine the attractive structural regularity of lithographically fabricated 3D porous carbon materials with the high surface-to-volume ratios of nanoscale pore metal structures, and allow for high mass transport access and catalytic activity for a diverse range of applications, ranging from fuel cells to chemical sensors. These attractive features and advantages are described below using a biofuel cell constructed with the new hierarchical structure compared to the one based on the microporous carbon surface.

2. Experimental section

2.1 3D porous substrate preparation

A porous carbon substrate with 3D nanostructure was obtained from Sandia National Lab (Sandia National Laboratories, Albuquerque, NM). 3D porous carbon electrodes were rinsed with isopropanol (Fisher Scientific, Fair Lawn, NJ) and ultrapure water followed by drying under N_2 stream. These porous carbon substrates were coated with Ti (20 nm) and Au layer (30 nm) using an E-beam evaporator (Temescal BJD 1800 E-beam Evaporator) as an adhesive layer for the nanoporous Au coating and were used as a working electrode for all experiments.

2.2 Nanoporous Au synthesis

The nanoporous Au film was synthesized employing an electrodeposition and sputtering technique. The mixtures of gold and silver plating solution (Orotemp 24 RTU RACK and 1025 RTU@4.5 Troy/Gallon) (85/15 ratio) were used for electrodeposition processes. The three deposition potentials were demonstrated (−0.5 V, −0.75 V and −1.0 V) and two deposition times were investigated (120 and 300 s). The potential was controlled by a μ-Autolab type II (Eco Chemie, Utrecht, The Netherlands) and a conventional three-electrode electrochemical cell. A platinum wire was used as a counter-electrode and Ag/AgCl (in 1 M KCl) was used as a reference electrode. The ability to tailor nanoporous structure using different plating ratios (5/5, 6/4, 7/3 and 8/2) and constant deposition potential (−0.9 V, 300 s) was also employed. All plating solution in this work was diluted with ultrapure water in the ratio of 1 : 1 before use. The silver component was etched (dealloyed) using HNO_3 (70%) for 15 min and the porous structure was thoroughly rinsed with ultrapure water. To generate nanoporous Au using the sputtering technique, the Denton Discovery 18 was used. The compositions of alloys were co-sputtered onto the PC substrate using different Au and Ag target gun power settings. DC power for Au was 100 and 150 W, RF power for Ag was 400 and 350 W, respectively. The sputter was performed at room temperature under vacuum of 5×10^{-6} Torr and flow Ar to 3.6 mT. Au shutter was opened 30 s before Ag shutter. The rotation speed was 65. The sputter time was 3 min.

2.3 Nanoporous Ag synthesis

The ability to generate nanoporous Ag was also presented here using the sputtering technique. The fabrication processes were carried out at room temperature under a vacuum of 5×10^{-6} T, and flow Ar to 3 mT. The Ag shutter was opened 100 s before the Al shutter. The sputter time was 20 min. The DC power for Al was 120 W and RF power for Ag was 50 W. The film was etched in H_2SO_4 (1 M, 2 h).

2.4 Characterization

Scanning electron microscopy (SEM) images were taken using a Phillips XL30 ESEM instrument using an acceleration potential of 20 kV. Metal compositions were qualified by Oxford EDX attached to the SEM instrument and operated by Inca software. The electrochemical active surface area of the nanoporous gold was determined from cyclic voltammogram by the scanning nanoporous gold electrode in a N_2-saturated H_2SO_4 (0.1 M) (Fisher Scientific, Fair Lawn, NJ) at a scan rate of 50 mV s^{-1} to measure the charge integration under oxide reduction peak and compared to the electrochemical active surface area of the alloy one.

2.5 Biofuel cell construction

The nanoporous gold-modified 3D porous carbon employed as a bioanode was prepared by depositing the Au–Ag alloy using

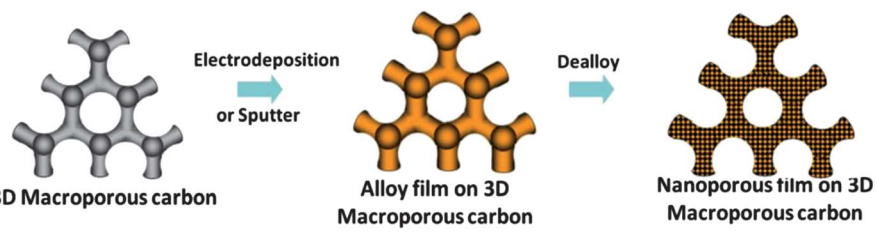

Fig. 1 Creation of bicontinuous nanoporous surfaces along with a large open-pore macrostructure on highly ordered 3D porous carbon using bimetal alloy deposition followed by chemical etching of less noble metal.

a deposition potential of −0.75 V for 3 min and an 85/15 (Au/Ag) ratio. The film was then dealloyed in 70% HNO_3 for a time of 15 min. The Meldola's blue-glucose dehydrogenase (MDB-GDH)-modified anode was fabricated by immersing the nanoporous Au-3D PC into a MDB solution for 30 min, followed by casting 4.5 μL of GDH (2 U μL^{-1}) mixed with 1% BSA (the mixed ratio 2 : 1) on the electrode, and dropping 6 μL of 40 mM glutaraldehyde. The biofuel cell cathode was prepared by electrodepositing Pt nanoparticles onto a Pt disk electrode from a plating solution containing 4 mM H_2PtCl_4 in 0.5 M H_3BO_3 using a deposition potential of −0.3 V for 180 s. Phosphate buffer (0.1 M, pH 7.0) containing 20 mM NAD^+ was used as an electrolyte and glucose (30 mM) was used as a fuel.

3. Results and discussion

3.1 Preparation of nanoporous metal decorated 3D microporous carbon substrate

Initial attempts to prepare hierarchical structures involved the creation of a nanoporous silver film on the multilayered microporous carbon through sputtering of a binary Ag–Al alloy followed by the dealloying the Al using 1 M H_2SO_4 for 2 h. The formation of the pores during the dealloying process involved etching of the less noble metal causing surface diffusion of the nobler element along the alloy–electrolyte interface.[13–17]

Fig. 2 displays scanning electron microscopy (SEM) images of the preparation of the nanoporous silver onto a lithographically patterned highly ordered porous carbon. Fig. 2A shows the bare porous carbon substrate before depositing the Ag–Al alloy. The pore diameter is noted to be 890 nm. The corresponding image after sputtering the alloy is shown in Fig. 2B. This SEM image indicates that the coverage of the Ag–Al sputtered film over the carbon surface is relatively homogeneous, resulting in a pore diameter of 700 nm. EDX analysis indicates Ag and Al atomic contents of 35% and 65%, respectively. Cross-section images from previous studies on silver sputtered films onto the same substrates showed that the sputtering process is not simply line-of-sight and produces coatings on undersides as well, most likely due to the open nature of the structures.[18] Fig. 2C shows the image of the nanoporous silver film after etching the aluminium, and displays a maze-like morphology of nanopores and ligaments, characteristic of the dealloying process. The Al dissolution leaves behind a nanoporous Ag with interconnected pore characteristics, closely resembling natural sea coral. The resulting nanoporous Ag film has an average pore size of about 32 nm and ligament widths of 70 nm. The overall structure has a micropore diameter of 790 nm. Such an increase in the micropore diameter, from the alloy film (700 nm) to the dealloyed film (790 nm), reflects the variation of microstructure porosity through the Ag-reordering process. Overall, these examinations reveal that an ultra-rough Ag nanocoral structure can be prepared from an aluminium-rich Ag–Al alloy film and could be extended to different Ag–Al alloy ratio films to tune the nanoporosity, thickness and ligament size.

Subsequent studies focused on the formation of nano- and micro-pores by coated nanoporous gold onto the 3D macroporous carbon through vapor deposition as well as co-electrodeposition of a binary Au–Ag alloy. The formation of the Au–Ag alloy films over the 3D substrate penetrated into 3 layers of the microporous carbon, as was observed previously using this technique,[18] unlike electrodeposition of Pt nanoparticles from previous studies.[19] After dealloying in 70% HNO_3 for 15 min silver undergoes depletion not only on the surface but at appreciable depths within the film, leading to the reordering/coarsening of the Au adatoms into island growth and nucleation.[4,13–17] The sponge-like morphology of the resulting nanoporous gold consists of interconnecting ligaments with diameters on the order of tens of nanometres (exact dimensions discussed in next sections). A nanoporous Au structure of uniform pore size and distribution, closely resembling the highly rough morphology of cauliflower, is thus observed. The film thickness for each deposition method was measured before and after Ag dissolution. This thickness does not change significantly after the dealloying process. Hence, a negligible variation in the microporosity between the alloy and dealloy films is also observed, with a small (3%) increase in diameter for the sputtered sample and a 2% increase for the electrochemically deposited sample.

3.2 Tailoring nano/microporosity

Due to self-diffusion and rearrangement of Au atoms at the electrolyte–metal interface,[13,14,16,20,21] the Au ligaments were tailored through control of the dealloying time. Fig. 3 displays SEM images of the nanoporous Au on the 3D porous carbon obtained from electrodeposition of Au/Ag (85/15) plating solution and deposited at −0.75 V for 180 s followed by dealloying in 70% HNO_3. Increasing the dealloying times from (A) 15 min to (B) 15 h and (C) 30 h allows a significant increase in coarsening of the Au adatoms, resulting in enlargement of the Au ligament from 10 nm to 40 nm.

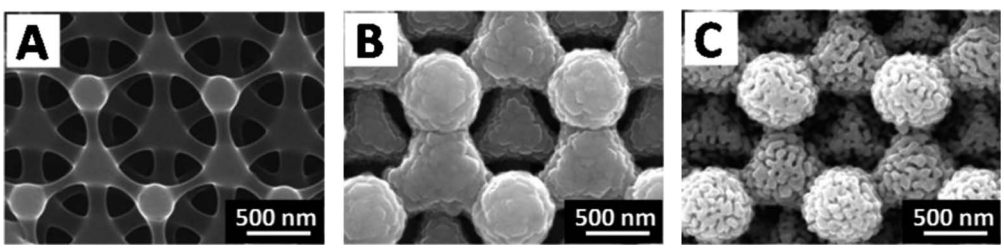

Fig. 2 Creation of nanoporous surfaces on a large open-micropore structure using sputtering of an Ag–Al alloy film followed by chemically dealloying of the Al component to transform dense film to bicontinuous nanoporous film. *Conditions*: Sputtering time 20 min for Ag–Al alloy film and dealloying using 1 M H_2SO_4 for 2 h. (A) Porous carbon, (B) Ag–Al alloy film and (C) porous Ag on 3D porous carbon.

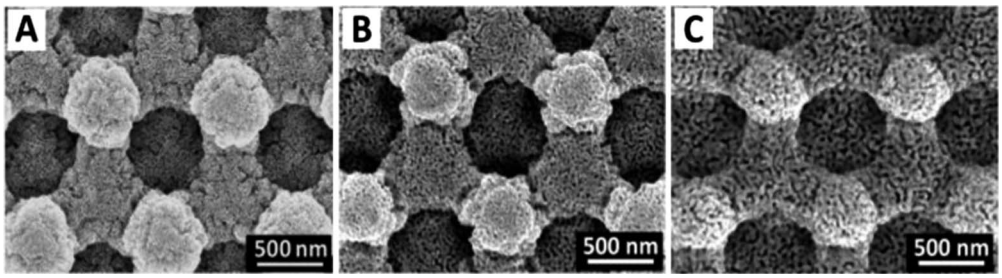

Fig. 3 SEM images of nanoporous Au on 3D porous carbon at different dealloying times, (A) 15 min, (B) 15 h and (C) 30 h, using Au_{85}–Ag_{15} plating solution and deposited at −0.75 V for 180 s.

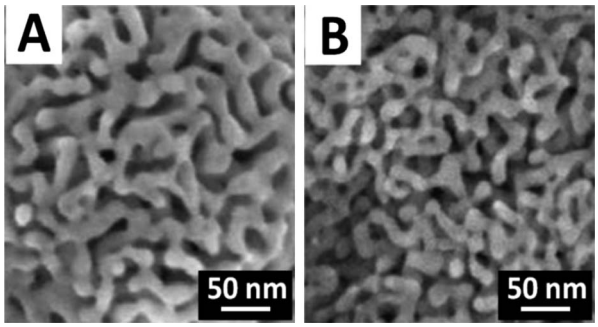

Fig. 4 Creation of nanoporous Au surfaces using (A) sputtering and (B) electrodeposition of bimetallic alloy (Au–Ag) film on highly ordered 3D porous carbon followed by chemically dealloying less noble metal (Ag).

Fig. 4 displays close-up images of the morphology of the nanoporous gold on the 3D macroporous carbon substrate, prepared from both sputtering and electrodeposition techniques. Sputtering of the Au–Ag alloy film (10 min) followed by dealloying leads to a nanoporous Au film, outlined in Fig. 4A.

Such sputtering conditions offer unimodal pore sizes in the range of 10–20 nm and ligament networks with widths in the range of 15–30 nm. Fig. 4B displays SEM images of nanoporous Au prepared by a 5 min electrodeposition at −0.75 V from the mixture of Au and Ag plating solution at the ratio of 85/15, and dealloying the Ag using 70% HNO_3 for 15 min. Such an image shows a sponge-like nanoporous structure with unimodal pore size in the range of 7–20 nm and ligament network with ligament widths in the range of 10–20 nm, resembling a nanocoral-like structure.

In this work, however, the electrochemically deposited alloy displays a rougher morphology with higher porosity than that of the sputtered substrate which should be more favorable for many applications. The higher density of pores and interconnectivity can be attributed to a more homogeneous layer of alloy formed during electrodeposition. In the following sections we will discuss the influence of different Au/Ag ratios, electrochemical deposition potentials, film shrinkage after the dealloying step and characterization of the morphology of each substrate for a variety of experimental conditions.

The nanoporosity of bicontinuous metal films over the 3D porous carbon substrate can be tailored through the variation of the deposition potential that leads to the formation of alloy films with different metal compositions. The ability to control metal contents in the alloy film was investigated and the results are illustrated in Fig. 5. The experiments were carried out over a potential range of −0.5 to −1.25 V using a 3 min deposition time and an Au–Ag mixture (ratio of 85/15). The different reduction rates of silver and gold at different deposition potentials lead to varying Au and Ag compositions[13,14,16,20,21] and hence a porous film with varying pore sizes and film thicknesses. The alloy film and the pore morphology at plating potentials of −0.5, −0.75 and −1.0 V were characterized with SEM (data not shown here) and EDX analysis (shown in Fig. 5D). The resulting EDX analysis indicated that the alloy film contained 7.5%, 28% and 40% atomic gold for deposition potentials of −0.5, −0.75 and −1.0 V, respectively.

After the dealloying, wide open pores with thin network connections are observed for a deposition potential of −0.5 V, shown in Fig. 5A. The decrease in the film thickness, from 300 nm for the alloy film to 100 nm for the dealloyed porous film, is noteworthy, and is attributed to the high Ag content of up to 91 atomic%, and the concomitant coarsening of the Au adatoms into a thin porous film. This has the effect to increase the micropore diameter from 650 nm (alloy) to 850 nm (dealloy). Pore sizes in the range of 13–40 nm and ligament sizes in the range of 4–12 nm are observed. A high relative range in pore size as well as a large maximum diameter and small ligament size are observed for this deposition potential.

The corresponding dealloyed nanoporous structure at −0.75 V is displayed in Fig. 5B. The morphology shows a much more highly ordered porosity than that observed in Fig. 5A, and is more characteristic of the sponge-like nanoporous gold. A minimal change in the film thickness (and thus the micropore diameter) is observed before and after the dealloying step, reflecting a higher percentage of Au in the mixture. A coral-like homogeneous structure was achieved with pore sizes in the range of 7–20 nm and ligaments sizes in the range of 10–20 nm. This reflects the larger extent of gold co-deposition at more negative potentials associated with the different standard reduction potentials of the silver and gold plating solutions. Finally, the image in Fig. 5C shows the morphology of the dealloy film at a deposition potential of −1.0 V which corresponds to 40 atomic % Au (EDX analysis, Fig. 5D).

The pore formation is less dense with smaller sizes than those previously observed in Fig. 5A and B, yielding pore sizes in the range of 4–8 nm and ligaments sizes in the range of 12–32 nm. However, solid crystalline features still remain on the film surface and thus little nanoporosity is observed. The ligament size varies substantially due to the presence of solid crystals and thus ligament widths calculated are not reflective of an actual structure with high porosity. As with Fig. 5B, a minimal change in the film

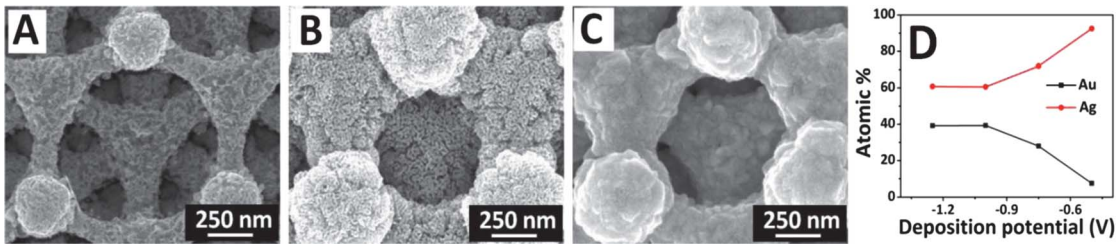

Fig. 5 SEM images of a nanoporous Au film on 3D porous carbon using Au_{85}–Ag_{15} plating solution deposited for 180 s at different deposition potentials: (A) −0.5 V, (B) −0.75 V, (C) −1.0 V, dealloying 15 min in 70% HNO_3, and (D) EDX analysis showing metal compositions in the alloy film at different deposition potentials.

thickness and thus of the micropore diameter is observed due to the higher percentage of Au present in the alloy compared to that in Fig. 5A. These images show that control of ligament size can be achieved by increasing the percentages of gold deposited onto the carbon surface which is achieved by varying the metal precursor concentration. The atomic% Au is always lower than Ag due to the more negative reduction potential of the Au compared to that of Ag. The increase in the Au content (*i.e.* lower Ag content) at higher deposition potentials is clearly reflected through a significant decrease in porosity attributed to a lower need for reordering of Au during the dealloying step.

Tailoring nano/microporosity with alloy ratios of the plating solution which allows tuneable morphology was also investigated. Here, nanoporous Au films of varying thicknesses were obtained from Au–Ag solution mixtures with different ratios (using a potential of −0.9 V for 5 min) 6/4, 7/3, and 8/2. However, the pore sizes and distributions of nanoporous Au are noticeably unchanged at approximately 7–20 nm for each sample and ligament sizes were 10–20 nm. The nanoporous structure itself retains its nanocoral-like features, thus retaining the remarkably high surface-to-volume ratios and self-supporting characteristics (SEM images not shown here). The EDX analysis of alloy films displays the atomic percentages of $Au_{27}Ag_{73}$, $Au_{34}Ag_{67}$, and $Au_{49}Ag_{51}$. Interconnected nanoporous Au can be fabricated from Ag-rich film having Ag content about 60–90% (10–40 atomic% Au). Outside of these ranges (>40% and <10% Au) the sponge-like nature of the nanoporous film was not observed.

3.3 Electrochemical characterization of nanoporous gold electrodes for varying deposition potentials

Cyclic voltammetry was used to characterize the electrochemically active surface area (ECSA) of nanoporous gold structures prepared at different electrochemical deposition potentials, as well as for a nanoporous gold substrate formed by co-sputtering. In these experiments, the surface area of the nanoporous gold electrodes was examined in 0.1 M H_2SO_4 solution. The CV was scanned over a potential range of 0.0 to 1.5 V (*vs.* Ag/AgCl) at a scan rate of 50 mV s^{-1}. The resulting cyclic voltammograms, shown in Fig. 6, are characteristic of the oxidation of gold in this acidic solution, whereby an oxidation signal is observed for the anodic scan due to the formation of gold oxide and a reduction signal for gold oxide is observed at a potential of −0.75 V on the reverse scan. This characteristic signal was observed for the following nanoporous Au electrode surfaces prepared from: (a) sputtering using gun power 100 W, and electrodeposited at

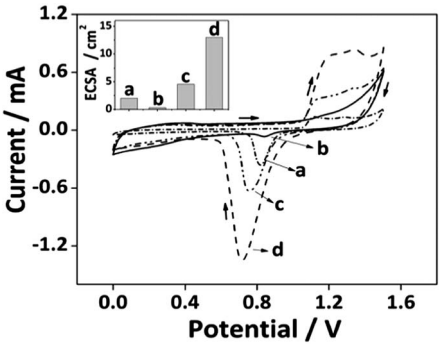

Fig. 6 CV of nanoporous gold on a 3D porous carbon electrode in 0.1 M H_2SO_4 with a scan rate of 50 mV s^{-1}; (a) Au-modified 3D-porous carbon using the sputtering technique compared with nanoporous Au prepared using the electrodeposition technique at deposition potentials of (b) −0.5 V, (c) −0.75 V and (d) −1.0 V; inset displays ECSA of nanoporous Au at different prepared conditions.

potentials (b) −0.5 V, (c) −0.75 V and (d) −1.0 V. It is clear that the magnitude of the Au oxide reduction signal increases with increasingly negative deposition potentials. The increase in this signal is attributed to the increase in the overall electrochemically active surface area of the electrode. The ECSA was calculated by integrating the charge under the reduction signal using a GPES software and assuming a specific charge of 386 μC cm^{-2} for Au oxide reduction.[7,22] The inset of Fig. 6 displays ECSA of nanoporous Au under different prepared conditions. The increasing value of the Au oxide reduction signal in Fig. 6, upon changing the deposition potential from −0.5 V to −0.75 V and then to −1.0 V, is expected. The film thickness for the latter two electrode surfaces was greater than that of the former, in accordance with the presence of substantially more surface area. The increase in ECSA from a deposition potential of −0.75 V to −1.0 V is also noteworthy since the sample deposited at −0.75 V shows clearly more porous features to that deposited at −1.0 V. However, the sub-surface porosity is not clearly visible from the SEM image along with EDX (Fig. 5) and CV shows that the Au loading at −1.0 V is higher than at −0.75 V. The ECSA value for the sputtered substrate is 2 cm^2 and it is in between that of the electrochemically deposited samples at −0.5 and −0.75 V. The porosity of the sputtered substrate shows a much more crystalline morphology in many areas of the sample, with an overall less exposed active area of the gold.

The ESCA values increase from 0.3, 4.5 and 13.0 cm^2 at a deposition potential of −0.5, −0.75 and −1.0 V. This outlines

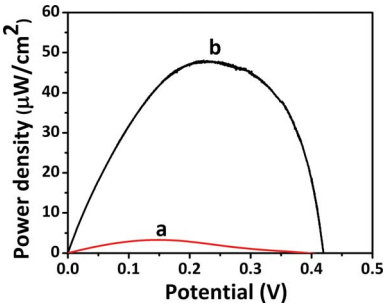

Fig. 7 Power density curves of (a) (GDH-MDB)-modified 3D microporous carbon electrode and (b) a (GDH-MDB)-modified 3D nano/micro-porous electrode in 0.1 M PBS (pH 7.0) containing 20 mM NAD^+ and 30 mM glucose.

the major advantage of the incorporation of a highly developed three-dimensionally interconnected porous network of micro- and nano-pore films, compared to the two-dimensional flat polycrystalline electrode. The largest enhancement of the nanoporous gold is observed for a deposition potential of −1.0 V, which shows a 108-fold enhancement over the planar Au disk electrode (ESCA 0.12 cm^2). The large utilization of Au in the other samples is attributed to the synergy effect of nanoporous gold on the microporous carbon displaying the extremely high surface-to-volume ratios that can be achieved using the dealloying method of a binary metal mixture.

3.4 Biofuel cell application

The functionality and advantages of the new 3D hierarchical nano/microporous architectures were illustrated for a greatly enhanced performance of an enzymatic biofuel cell compared to the bare 3D carbon macroporous carbon. For this purpose we constructed for the first time a biofuel cell system employing hierarchical nanoporous Au-modified microporous carbon structures by coating it with a Meldola's blue-glucose dehydrogenase (MDB-GDH) layer. First, MDB was coated onto a 3D hierarchical nano/microporous substrate, followed by immobilization of GDH using glutaraldehyde as a cross-linker. The resulting 3D bioelectrocatalytic electrode provides both nanopores to support the biocatalytic sites and micropores to support effective mass transport of the glucose fuel. As a result, and as illustrated in Fig. 7, the new 3D bioelectrocatalytic nano/microporous anode, coupled to the Pt nanoparticle-modified Pt disk cathode, provided a high power density output of 45 μW cm^{-2}, with the open circuit voltage of 0.46 V, which is 10 times larger than the power observed at the MDB-modified 3D microporous carbon surface (4 μW cm^{-2}). This new 3D hierarchical nano/microporous architecture can be extended for a wide range of applications in sensor technology to energy applications.

4. Conclusions

In conclusion, we have demonstrated the formation of hierarchical nanoporous Au and Ag structures on a microporous lithographically defined 3D multilayered carbon scaffold from the deposition of a binary alloy (*e.g.*, Au–Ag and Ag–Al) followed by etching of the Ag and Al, respectively. The dissolution and reordering processes result in the formation of nanopores in combination with microporous substrates with unique surface morphologies, leading to highly nodular cauliflower- and coral-like nanostructures. We have illustrated the ability to tailor the thickness and porosity of monolithic nanoporous gold along with the control of the microporous architecture through controlled electroplating conditions *i.e.*, deposition potentials and plating solutions. Such a fine control of the physical characteristics of the resulting nanoporous gold film reflects the different extents of gold-reordering during the coarsening process. The deposition of such variable nanoporous films onto the microporous carbon substrate combines the high surface-to-volume ratio and favorable catalytic characteristics of nanoporous gold with the open-cell morphology of carbon foams to offer many structural and hydrodynamic advantages compared to common nanoporous metal structures on planar surfaces. Finally, we demonstrated the enhanced functionality of the new 3D hierarchical nano/microporous architectures toward biofuel cell systems, where the new 3D bioelectrocatalytic anode provided a substantially higher power density output (45 μW cm^{-2}) compared to the corresponding 3D microporous carbon substrate. These bioinspired hierarchical coral- and cauliflower-like nanostructures hold also considerable promise for Surface-Enhanced Raman Spectroscopy (SERS)[23] chemical and biological sensing, as well as to future electronic and energy-storage devices.

Acknowledgements

This work was supported by the Laboratory Directed Research and Development program at Sandia National Laboratories and the National Science Foundation (Award Number CHE-1057562). A.O' M. was partially supported by DOE BES DE-SC0004937.

Notes and references

1 J. E. G. J. Wijnhoven, S. J. M. Zevenhuizen, M. A. Hendriks, D. Vanmaekelbergh, J. J. Kelly and W. L. Vos, *Adv. Mater.*, 2000, **12**, 888.
2 J. Zhang, Y. Li, X. Zhang and B. Yang, *Adv. Mater.*, 2010, **22**, 4249.
3 J. Erlebacher, M. J. Aziz, A. Karma, N. Dimitrov and K. Sleradzki, *Nature*, 2001, **410**, 450.
4 Y. Ding and J. Erlebacher, *J. Am. Chem. Soc.*, 2003, **125**, 7772.
5 Y. Yu, L. Gu, X. Lang, C. Zhu, T. Fujita, M. W. Chen and J. Maier, *Adv. Mater.*, 2011, **23**, 2443.
6 S. Ahl, P. J. Cameron, J. Liu, W. Knoll, J. Erlebacher and F. Yu, *Plasmonics*, 2008, **3**, 13.
7 (*a*) S. Ben-Ali, D. A. Cook, S. A. G. Evans, A. Thienpont, P. N. Bartlett and A. Kuhn, *Electrochem. Commun.*, 2003, **5**, 747; (*b*) S. Campuzano and J. Wang, *Electroanalysis*, 2011, **23**, 1289.
8 R. Szamocki, S. Reculusa, S. Ravaine, P. N. Bartlett, A. Kuhn and R. Hempelmann, *Angew. Chem., Int. Ed.*, 2006, **45**, 1317.
9 A. Wittstock, V. Zielasek, J. Biener, C. M. Friend and M. Bäumer, *Science*, 2010, **327**, 319.
10 V. Zielasek, B. Jürgens, C. Schulz, J. Biener, M. M. Biener, A. V. Hamza and M. Bäumer, *Angew. Chem., Int. Ed.*, 2006, **45**, 8241.
11 D. B. Burckel, C. M. Washburn, A. K. Raub, S. R. J. Brueck, D. R. Wheeler, S. M. Brozik and R. Polsky, *Small*, 2009, **5**, 2792.
12 X. Xiao, M. E. Roberts, D. R. Wheeler, C. M. Washburn, T. L. Edwards, S. M. Brozik, G. A. Montaño, B. C. Bunker, D. B. Burckel and R. Polsky, *ACS Appl. Mater. Interfaces*, 2010, **2**, 3179.

13 C. Ji and P. C. Searson, *Appl. Phys. Lett.*, 2002, **81**, 4437.
14 C. Ji and P. C. Searson, *J. Phys. Chem. B*, 2003, **107**, 4494.
15 A. J. Forty, *Nature*, 1979, **282**, 597.
16 R. Laocharoensuk, S. Sattayasamitsathit, J. Burdick, P. Kanatharana, P. Thavarungkul and J. Wang, *ACS Nano*, 2007, **1**, 403.
17 Z. Zhang, Y. Wang, Z. Qi, W. Zhang, J. Qin and J. Frenzel, *J. Phys. Chem. C*, 2009, **113**, 12629.
18 X. Xiao, J. Nogan, T. Beechem, G. A. Montaño, C. M. Washburn, J. Wang, S. M. Brozik, D. R. Wheeler, D. B. Burckel and R. Polsky, *Chem. Commun.*, 2011, **47**, 9858.
19 S. Sattayasamitsathit, A. M. O'Mahony, X. Xiao, S. M. Brozik, C. M. Washburn, D. R. Wheeler, J. Cha, D. B. Burckel, R. Polsky and J. Wang, *Electrochem. Commun.*, 2011, **13**, 856.
20 A. Bulbarello, S. Sattayasamitsathit, A. G. Crevillen, J. Burdick, S. Mannino, P. Kanatharana, P. Thavarungkul, A. Escarpa and J. Wang, *Small*, 2008, **4**, 597.
21 (*a*) C. Ji, G. Oskam, Y. Ding, J. D. Erlebacher, A. J. Wagner and P. C. Searson, *J. Electrochem. Soc.*, 2003, **150**, C523; (*b*) X. Hu, R. Wang, Y. Ding, X. Zhang and W. Jin, *Talanta*, 2010, **80**, 1737.
22 S. Trasatti and O. A. Petrii, *J. Electroanal. Chem.*, 1992, **327**, 353.
23 P. L. Stiles, J. A. Dieringer, N. C. Shah and R. P. Van Duyne, *Annu. Rev. Anal. Chem.*, 2008, **1**, 601.

